We are IntechOpen,
the world's leading publisher of
Open Access books
Built by scientists, for scientists

6,900
Open access books available

185,000
International authors and editors

200M
Downloads

154
Countries delivered to

Our authors are among the

TOP 1%
most cited scientists

12.2%
Contributors from top 500 universities

CLARIVATE ANALYTICS

BOOK CITATION INDEX

INDEXED

WEB OF SCIENCE™

Selection of our books indexed in the Book Citation Index
in Web of Science™ Core Collection (BKCI)

Interested in publishing with us?
Contact book.department@intechopen.com

Ultra-Wideband MM Wave System and RF Modules

Albert Sabban

Abstract

Compact wideband RF modules are crucial in mm-wave direction finding systems, radars, seekers, and communication systems. This chapter discusses new integrated wideband mm-wave RF modules. It also discusses the design and development of a compact wideband (18–40 GHz) frontend and a wideband (18–40 GHz) switch bank filter (SBF). The frontend electrical specifications determine the system signal-to-noise ratio and the system dynamic range. This chapter presents a low-cost integrated 18–40 GHz wideband compact frontend with a 47 dBm high power limiter. The frontend consists of two channels: a high gain and low gain channel. Wideband MMIC switches are employed to select the required channel. The gain of the high gain channel is around 27 dB with ±1 dB flatness. The noise figure of the module is around 9 dB. This chapter also presents a low-cost, integrated, 18–40 GHz wideband compact SFB module. The wideband SFB consists of three wideband side-coupled microstrip filters. The SFB MIMIC switches operate in the 18 to 40 GHz frequency range and are used to select the required filter. The insertion loss of each filter section is less than 11.5 dB ±1.5 dB. The novelty of this research is the development of compact, integrated wideband mm-wave RF modules for direction finding and communication systems.

Keywords: MM Wave Direction Finding System, Frontend, Filters, Wideband communication systems

1. Introduction

Design of wideband RF modules, filters, and antennas are presented in [1–12]. Wideband RF technologies such as MIC, MIMIC, and MEMS are presented in [1–7]. Wideband RF modules are crucial in the development of direction finding (DF) systems. A fully integrated 10–40 GHz superheterodyne receiver frontend using a 40–46 GHz IF is presented in [8]. Wideband RF technologies are used to develop wideband RF modules such as frontends, SFBs, and receiving and transmitting channels, as presented in [1–15]. A DF system measures the direction from which a received signal was transmitted. Radio DF is used in the navigation of ships, aircrafts, vehicles, and missiles to locate emergency transmitters for search and rescue, to locate illegal or interfering transmitters, and to track wildlife. The transmitted signal direction may be found by combining the direction information from two or more suitably spaced receivers by using triangulation. Triangulation is the process of determining the location of a point by forming triangles. Triangulation involves only angle measurements. A DF system provides the ability to locate the position of an enemy transmitter.

The demand for wide bandwidth makes the Ka band attractive for future commercial communication and the radar industry. Front-end modules, filter banks, and coupler modules are important units in radar, seekers, and communication systems. This chapter presents several wideband mm-wave RF modules. It also discusses the design and development of a compact wideband (18–40 GHz) frontend and a wideband (18–40 GHz) SBF. Advanced design system (ADS) full-wave electromagnetic software is used to develop wideband RF modules, as presented in [16].

2. Ultra-wideband direction finding system

Compact wideband RF modules are crucial in mm-wave direction finding, radars, seekers, and communication systems. **Figure 1** shows a compact 18–40 GHz DF system is shown. **Figure 2** presents the block diagram of a wideband mm-wave DF system. The DF system consists of SFB modules, frequency source unit, DF frontend modules, two omnidirectional frontend units, and downconverter units. Wideband RF technologies are used to develop wideband RF modules such as frontends, filters, and receiving and transmitting channels, as presented in [1–5]. Development of wideband filters, microwave components, RF modules, and antennas is widely discussed in the literature (see [1–14]).

2.1 Ultra-wideband compact MM-wave frontend1

Design and development of compact wideband frontend is crucial in development of DF systems. The RF modules and the system are designed using RF, ADS software, and momentum RF software, [16]. **ADS** is an electronic design automation software system. It offers complete design integration to designers of products such as cellular and portable phones, pagers, wireless networks, and radar and satellite communications systems.

ADS support communication systems and RF design engineers to develop all types of RF designs, from RF and microwave modules and printed antennas to
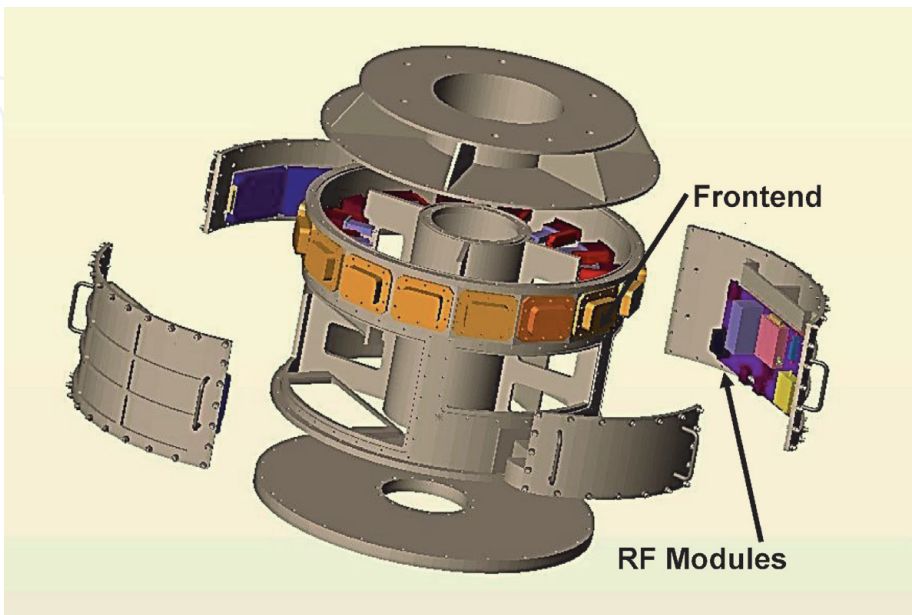

Figure 1.
Ultra-wideband DF system.

Figure 2.
Block diagram of an 18–40 GHz wideband DF system.

integrated MMICs for communication, medical, and aerospace defense applications as well as the Internet of Things (IoT).

With a complete set of simulation technologies ranging from frequency and time domain circuit simulation to electromagnetic field simulation. ADS let designers fully characterize and optimize designs, such as harmonic balance, circuit envelope, transient convolution, ptolemy, X-parameter, momentum, and 3D EM simulators (including both FEM and FDTD solvers). Measured results approve the computed results and the design process.

2.2 Compact MM-wave frontend requirements

Table 1 lists the frontend electrical specifications. The frontend design presented in this section meets the frontend electrical specifications. **Figure 3** presents the frontend block diagram, and **Table 2** lists the frontend interface connectors.
    Physical characteristics - interface connectors

2.3 Wideband front-end design

Figure 3 shows a frontend block diagram. The frontend module consists of a limiter and a wideband 18–40 GHz low noise amplifier (LNA) LMA406. The solid state LMA406 is a low noise PHEMT amplifier that operates from 18 to 40 GHz. The amplifier is a two-stage amplifier.

The amplifier gain is around 12 dB with 4.5 dB noise figure and 14 dBm saturated output power, and − 1 dB gain compression power output of +10 dBm. The LNA dimensions are 1.44 x 1.1 mm. A wideband PHEMT MMIC SPDT, AMMC-2008, was used. AMMC-2008 is a monolithic PHEMT SPDT switch with low insertion loss and high isolation from DC to 50 GHz. For improved reliability and moisture

Parameter	Requirements	Performance
Frequency range	18–40 GHz	Agree
Module gain	24 ± 3 dB, Switched by external control. (Lower than -40 dB for off state)	Agree
Module gain flatness	For any 0.5 GHz BW in 18–40 GHz ±0.5 dB max. For any 4GHz BW in 18–40GHz ±2 dB max. ±3 dB max for the whole range 18–40 GHz	Agree
High gain state noise figure	11 dB over temperature. 10 dB max for 40°C baseplate temperature.	Agree
Input power	−60 dBm to 10 dBm	Agree
Output power	13 dBm saturated −40 dBm to 11 dBm not saturated	Agree
Linearity	12 dBm min. Output at 1 dBc compression point 21 dBm single tone for third intercept point (Ip3) Second harmonic power − 25 dBc max. For 10 dBm output.	Agree
S11	Better than −9 dB	Agree
Input power protection	Input power 1 W CW at 0.1–40 GHz No damage at 1 W CW and 20 W Pulses Test for pulses: PW = 1 usec, PRF = 1KHz	Agree
Voltages	±5 V, +15 V	Agree
Control signals	LVTTL standard "0" = 0–0.8 V; "1" = 2.0–3.3 V	Agree
Switching time	Less than 0.1 usec	Agree
Output spurious, non-harmonic	When it is not, correlative with the input signals −50 dBm max.	Agree
Video leakage	Video leakage signals will be below the RF output level for terminated input	Agree
Module volume	6 x 4 x 2 cm	Agree

Table 1.
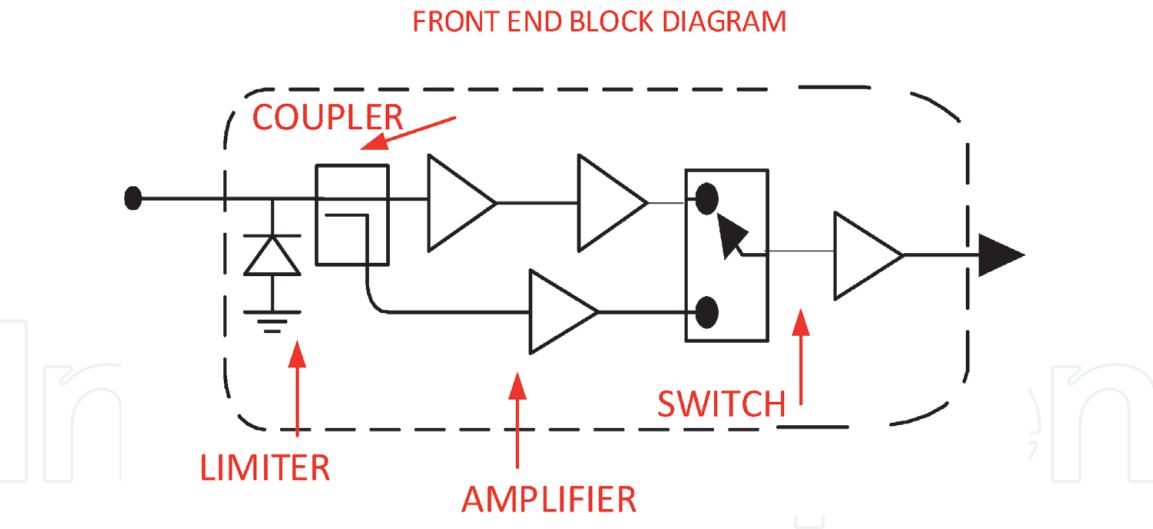*Electrical specifications of a wideband, 18–40GHz, DF frontend.*

Figure 3.
MM-wave frontend block diagram.

Interface	Type
RF input	Wave guide WRD180 (double ridge)
RF output	K connector
DC supply	D type
Control	D type

Table 2.
Interface connectors.

protection, the die is passivated at the active areas. One series and two shunt PHEMTs per throw provide 2.0 dB insertion loss and 28 dB isolation at 40 GHz. The isolation between the SPDT input port to the output ports is better than 25 dB. The SPDT 1 dBc compression point is around 14 dBm. The SPDT dimensions are 1 x 0.7 x 0.1 mm. The frontend electrical characteristics was evaluated using ADS Keysight software [15] and SYSCAL software. The MMIC amplifiers and the SPDT are connected to the surface of the mechanical box. The MMIC chips are assembled on a CoVar carrier. During development it was found that the spacing between the frontend carriers should be less than 0.03 mm to achieve flatness requirements and V.S.W.R better than 2:1.

Figure 4 presents the frontend block diagram used to calculate the module noise figure and gain. The LNA noise figure is 6 dB. The frontend calculated noise figure is 9.46 dB. The frontend gain is 21 dB. The computed frontend noise figure and gain for LNA noise figure of 5.5 dB is presented in **Figure 5**. The module computed noise figure is 9.25 dB, with 21 dB gain.

The frontend current and voltage consumption are given in **Table 3**. The frontend may operate in high gain state or in low gain state. The gain of the high gain channel is higher by 15 to 20 dB than the low gain channel. The frontend measured gain is presented in **Figure 6**. The measured gain is around 20 ± 4 dB at the frequency range of 18 to 40 GHz.

2.4 High gain wideband frontend module

To achieve a high gain frontend module a medium power MMIC amplifier, HMC283, was added to the frontend module as presented in **Figure 7**. The HMC283 chip is a medium power amplifier. The chip consists of a four-stage GaAs amplifier
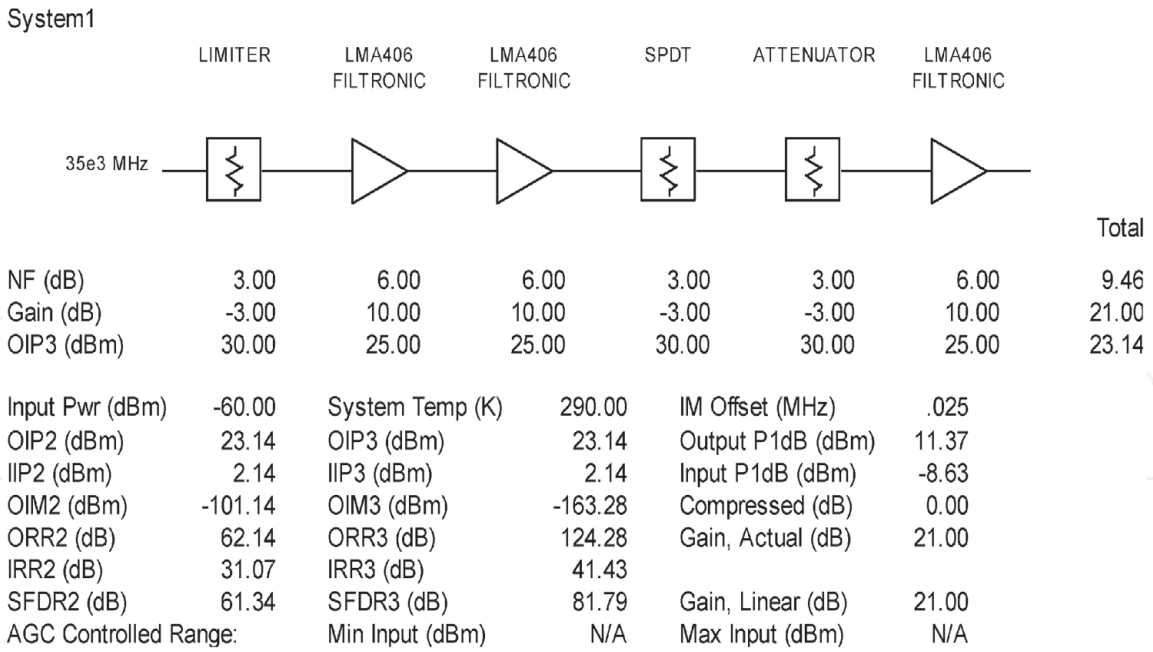
System1

	LIMITER	LMA406 FILTRONIC	LMA406 FILTRONIC	SPDT	ATTENUATOR	LMA406 FILTRONIC	Total
NF (dB)	3.00	6.00	6.00	3.00	3.00	6.00	9.46
Gain (dB)	-3.00	10.00	10.00	-3.00	-3.00	10.00	21.00
OIP3 (dBm)	30.00	25.00	25.00	30.00	30.00	25.00	23.14

Input Pwr (dBm)	-60.00	System Temp (K)	290.00	IM Offset (MHz)	.025	
OIP2 (dBm)	23.14	OIP3 (dBm)	23.14	Output P1dB (dBm)	11.37	
IIP2 (dBm)	2.14	IIP3 (dBm)	2.14	Input P1dB (dBm)	-8.63	
OIM2 (dBm)	-101.14	OIM3 (dBm)	-163.28	Compressed (dB)	0.00	
ORR2 (dB)	62.14	ORR3 (dB)	124.28	Gain, Actual (dB)	21.00	
IRR2 (dB)	31.07	IRR3 (dB)	41.43			
SFDR2 (dB)	61.34	SFDR3 (dB)	81.79	Gain, Linear (dB)	21.00	
AGC Controlled Range:		Min Input (dBm)	N/A	Max Input (dBm)	N/A	

Figure 4.
Frontend module design for LNA NF = 6 dB.

System1

	LIMITER	LMA406 FILTRONIC	ATTENUATOR	LMA406 FILTRONIC	SPDT	ATTENUATOR	LMA406 FILTRONIC	Total
NF (dB)	3.00	5.50	3.00	5.50	3.00	1.00	5.50	9.25
Gain (dB)	-3.00	10.50	-3.00	10.50	-3.00	-1.00	10.00	21.00
OIP3 (dBm)	30.00	25.00	30.00	25.00	30.00	30.00	25.00	23.61

Input Pwr (dBm)	-60.00	System Temp (K)	290.00	IM Offset (MHz)	.025	
OIP2 (dBm)	24.04	OIP3 (dBm)	23.61	Output P1dB (dBm)	11.74	
IIP2 (dBm)	3.04	IIP3 (dBm)	2.61	Input P1dB (dBm)	-8.26	
OIM2 (dBm)	-102.04	OIM3 (dBm)	-164.23	Compressed (dB)	0.00	
ORR2 (dB)	63.04	ORR3 (dB)	125.23	Gain, Actual (dB)	21.00	
IRR2 (dB)	31.52	IRR3 (dB)	41.74			
SFDR2 (dB)	61.90	SFDR3 (dB)	82.24	Gain, Linear (dB)	21.00	
AGC Controlled Range:		Min Input (dBm)	N/A	Max Input (dBm)	N/A	

Figure 5.
Frontend module design for LNA NF = 5.5 dB.

Voltage (v)	3	5	−12	−5	5 Digital
Current (A)	0.25	0.15	0.1	0.1	0.1

Table 3.
Wideband frontend module voltage and current consumption.

MMIC in the frequency range of 17 to 40 GHz. The chip dimension is 1.62 mm x 1.62 mm and may be integrated into multi-chip modules. The chip is a GaAs PHEMT amplifier with around 20 dB gain and + 21 dBm output power. The amplifier bias voltage is +3.5 V and consumes 300 mA of current.

The amplifier gain is around 21 dB with 10 dB noise figure and 21 dBm saturated output power. The amplifier dimensions are 1.72 x 0.9 mm. The high gain frontend module block diagram is shown in **Figures** 7 and **8**. The frontend module consists of high gain and low gain channels. **Figure** 7 presents the high gain and low gain channels without an amplifier in the low gain channel. **Figure 8** presents the high
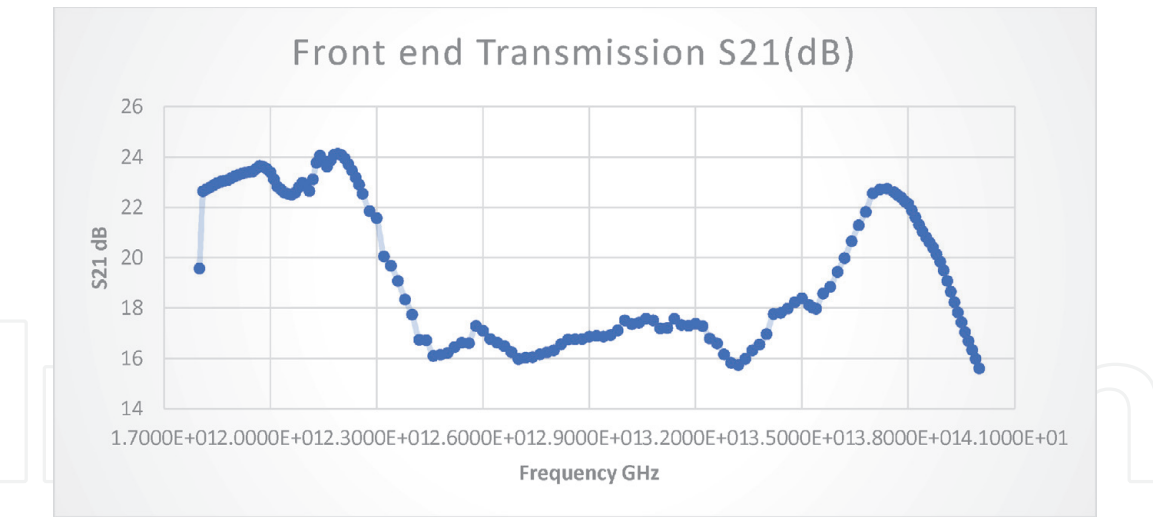
Figure 6.
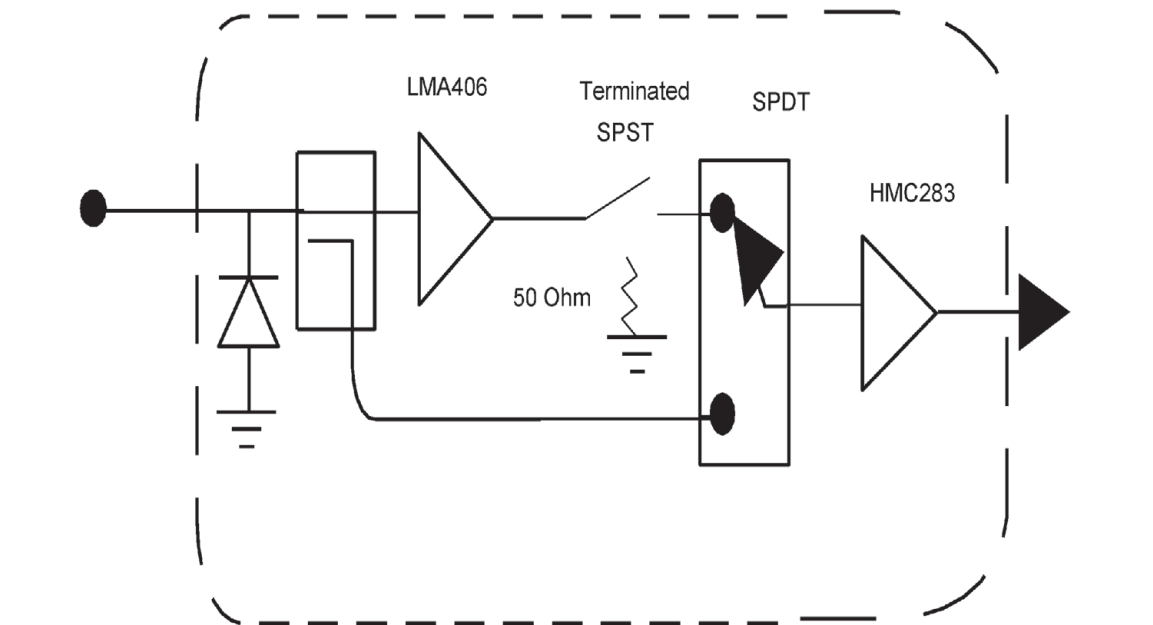*Measured wideband frontend gain 17 GHz to 40 GHz.*

Figure 7.
High gain frontend block diagram.

gain and low gain channels with an amplifier in the low gain channel. The gain difference between the high gain and low gain channels for the frontend presented in **Figure 8** is around 10 to 15 dB. Block diagram of the wideband frontend with one LMA406 amplifier in the high gain channel is shown in **Figure 9**.

2.5 High gain frontend design

The high frontend electrical characteristics were evaluated using ADS Agilent software and SYSCAL software. The calculated noise figure and gain for LNA noise figure of 9.5 dB is presented in **Figure 10**. The frontend calculated noise figure is 13.3 dB. The frontend gain is 32.5 dB. The frontend module calculated noise figure and gain for LNA noise figure of 5 dB is presented in **Figure 11**. The frontend calculated noise figure is 10 dB. The frontend gain is 29.5 dB.

Table 4 lists the measured results of frontend modules. **Figure 12** is a photo of HMC283 amplifier assembly, and **Figure 13** is a photo of the wideband compact frontend. **Table 5** provides the performance and cost of commercial mm-wave

FRONT END OPTION2
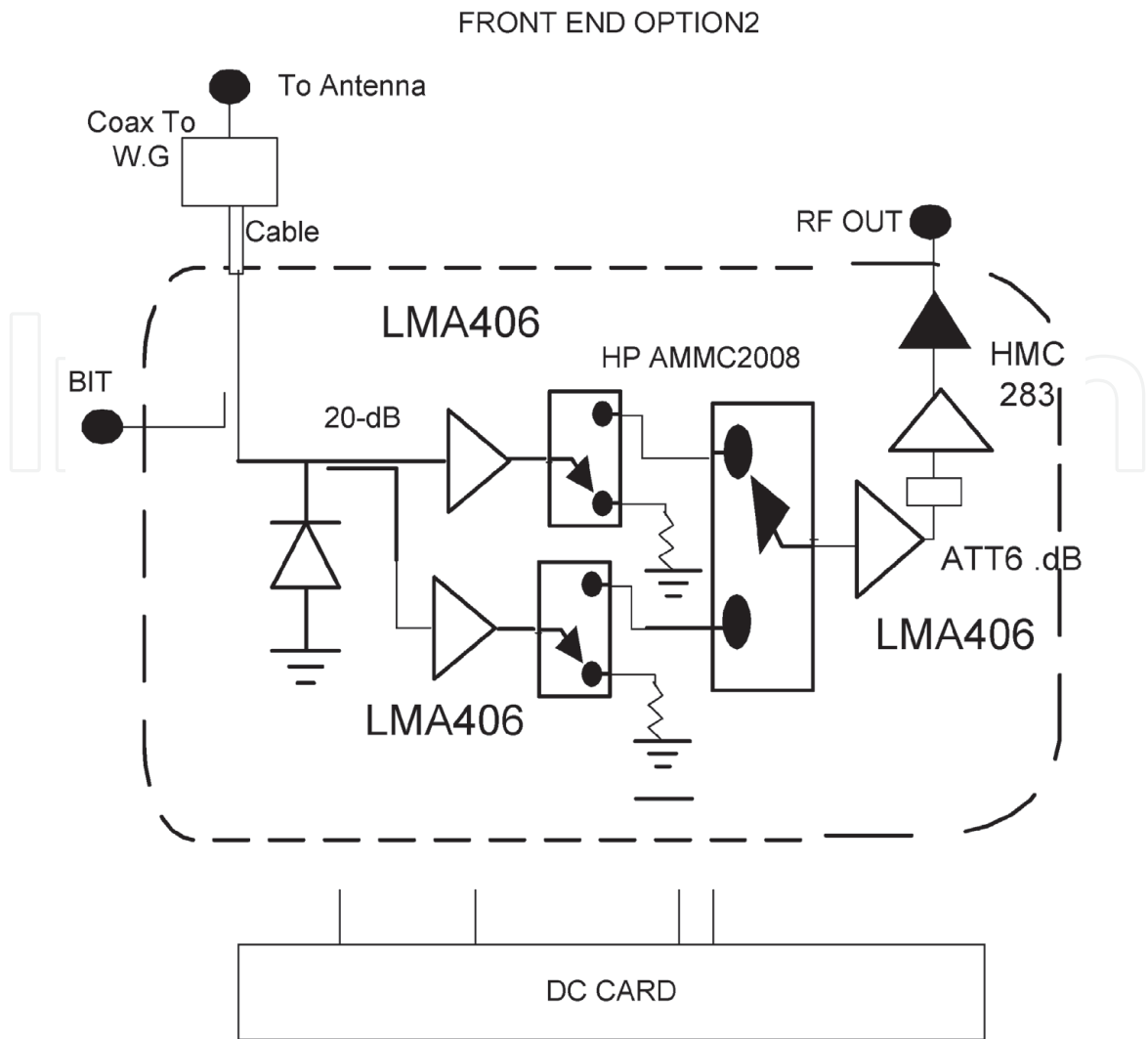
Figure 8.
High gain frontend block diagram with amplifier in the low gain channel.

FRONT END BLOCK DIAGRAM
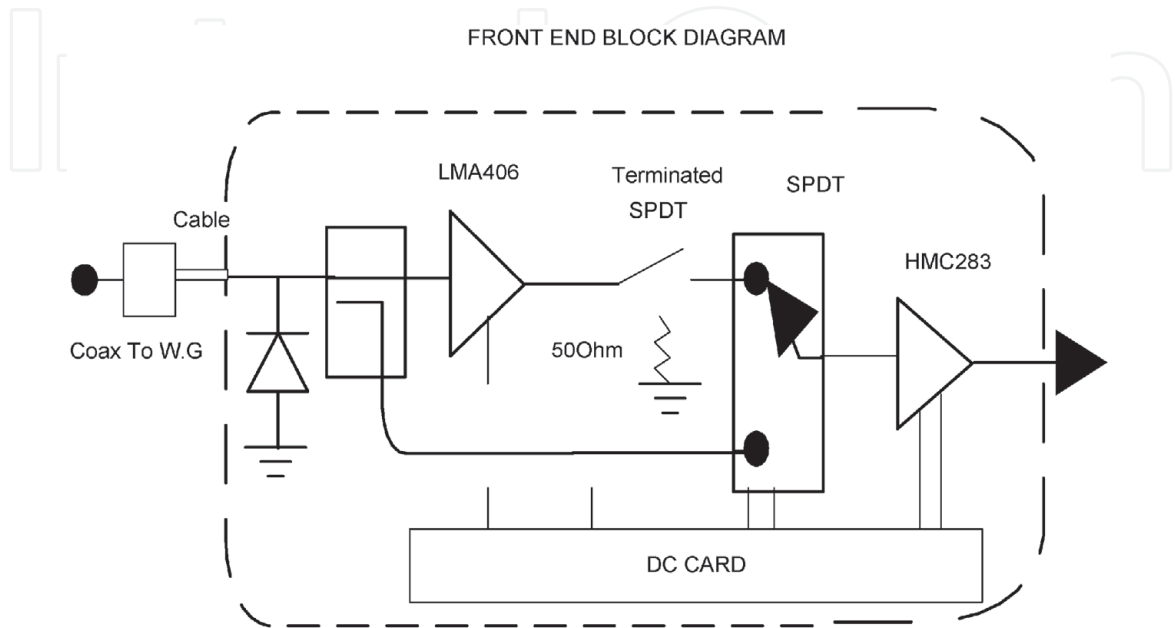
Figure 9.
Block diagram of the high gain wideband frontend with one LMA406 amplifier.

System1

	CONNECTOR +TRL+aduptor	limiter		cupler+trl	lmp406	2 spdt+TRL	lmp406	att	hmc283	Total
Gain (dB)	-3.00	0.50	9.50	-0.50	9.50	-6.00	9.50	-6.00	20.00	-0.70	32.48
OP1dB (dBm)	49.00	50.00	10.00	50.10	10.00	50.00	10.00	50.00	14.00	50.00	13.30
NF (dB)	3.00	0.50	5.00	0.50	5.00	6.00	5.00	6.00	13.00	0.70	8.94
Po (dBm)	-33.00	-32.50	-23.00	-23.50	-14.00	-20.16	-10.66	-16.82	3.18	2.48	
Pcomp (dB)	0.00	0.00	0.00	0.00	0.00	0.00	0.00	0.00	0.00	0.00	
NF+ (dB)	0.59		2.93		0.28	0.04	0.13	0.02	0.54		

Input Pwr (dBm) -30.00   System Temp (K)   298.00

Figure 10.
Wideband frontend module design for LNA NF =9.5 dB.

						Total
NF (dB)	3.50	5.00	5.00	5.00	6.00	9.00	10.02
Gain (dB)	-3.50	11.00	-5.00	11.00	-6.00	22.00	29.50
OIP3 (dBm)		20.00		20.00		20.00	19.87
NF+ (dB)		2.85		0.56		0.57	
Po (dBm)	-63.50	-52.50	-57.50	-46.50	-52.50	-30.50	

Input Pwr (dBm) -60.00   System Temp (K)   290.00
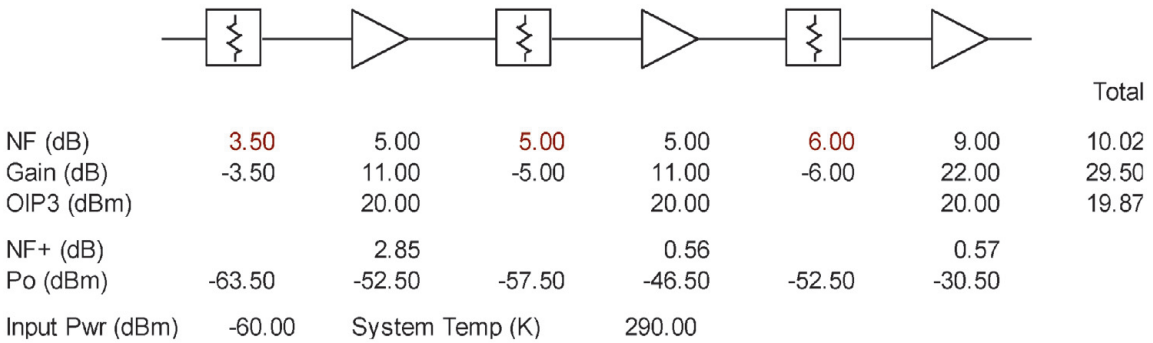
Figure 11.
Wideband frontend module design for LNA NF = 5 dB.

Parameter	OMNI02	OMNI01	DF6	DF4	DF3	DF2	DF1
Max. high gain mode	31.5	32	31	32	32.5	32.5	31
Min. high gain mode	28.5	28	26	26	27.5	27	26
Avg. high gain mode	30	30	29	29	29	29	29
Amplitude balance	3	4	5	6	5	5	4
S11 (dB)	5	4	4.5	5	5	5	5
S22 (dB)	7	6	7.5	6	5	6	5
Isolation (dB)	21.5	22.5	9	9	10	10	6.5
Max. low gain mode	16.5	18	19	18	17	17	17
Min. low gain mode	10.5	11	13	10	7.5	12	12
Avg. low gain mode	13.5	14.5	15	14	12	14	14
Amplitude balance	6	7	6	8	9.5	5	5

Parameter	OMNI02	OMNI01	DF6	DF4	DF3	DF2	DF1
P1 dBC 30 GHz	14	15.96	11.6	11.93	11.7	11.4	10.9
P1 dBC 40 GHz	14.48	16.8	13.96	14.5	15.58	15.28	14
NF 30 GHz	8.14	8.75	8.68	9.48	8.65	8.45	10.5
NF 40 GHz		8.75	9.28	10.1	8.64	9.17	10.24

Table 4.
Measured results of the wideband frontend modules.
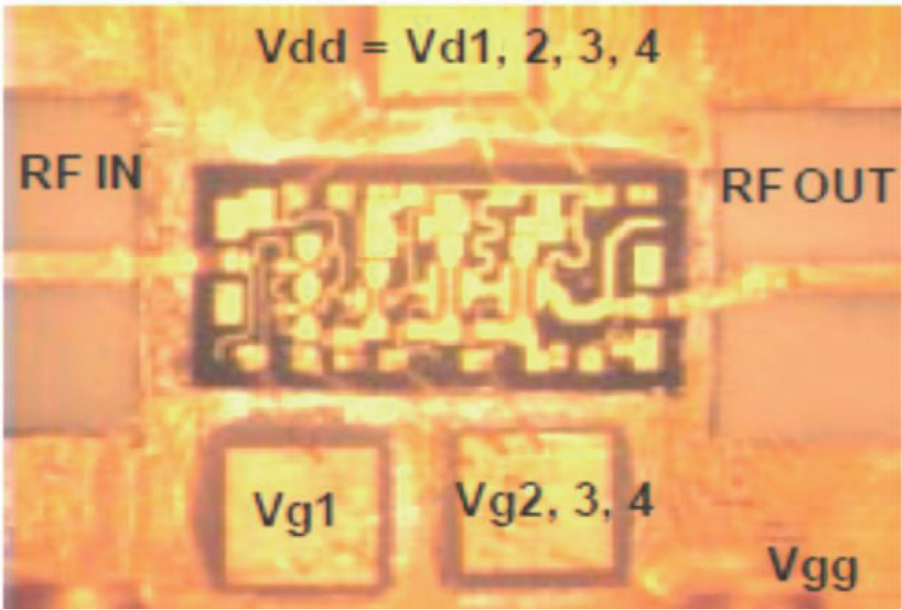
Figure 12.
Photo of HMC283 amplifier assembly.
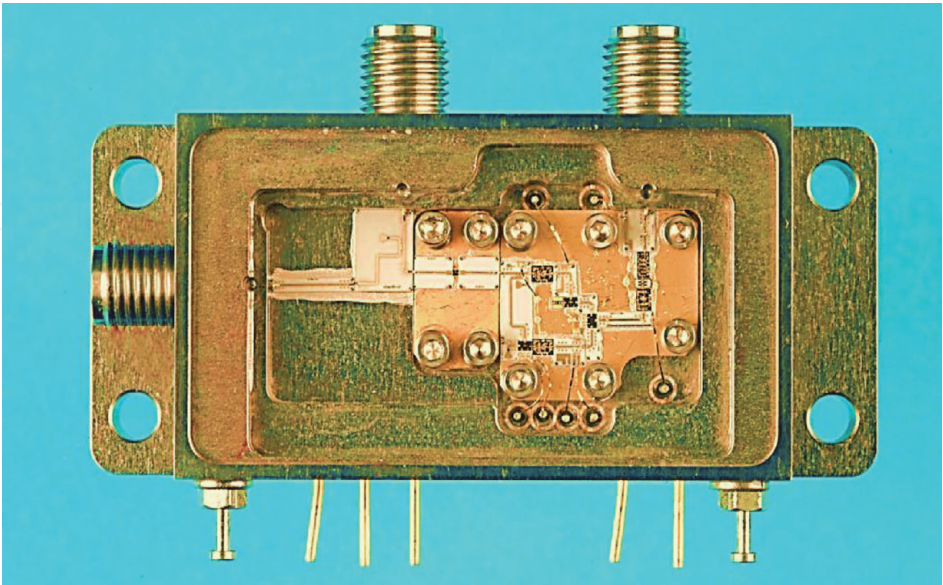
Figure 13.
Compact 18–40 GHz wideband frontend module.

microwave components. **Table 6** lists the costs of commercial MMIC and MIC mm-wave microwave components. There is a good agreement between computed and measured results. **Figure 14** is a photo of the compact mm-wave wideband, 18–40 GHz, frontend.

Component	Model#	Freq. [GHz]	NF / IL [dB]	Gain dB]	Power out 1dBc [dBm]	Coupling [dB]	Isolation [dB]	VSWR max	Unit Cost [K$]
Switch General Microwave	F9022	18–40	4	N/A		N/A	40	2.30:1	2.1
Coupler KRYTAR	184020	18–40	1.3	N/A		20		1.70:1	0.8
LNA Space Labs	SLKKa-30-6	18–40	6	30	17	N/A		1.80:1	2.2
WG/K Adapter MICROTEHC	R45 240130	18–40 18–40	0.75					1.25:1 1.6:1	0.5

Table 5.
Performance and cost of available connectorized mm-wave RF components.

Application	Component	Model#	TYPE	Unit Cost $
RF Frontend	Switch General Microwave	F9022	Drop in	1800
RF Frontend	LNA Filtronic	LMA406	MMIC	24
RF Frontend	LNA/VGA UMS	CHA2097A	MMIC	42
RF Frontend	Limiter Diode	GC4800	Diode	100
SFB	Switch	HMMC2027 HP	MMIC	80
SFB	Switch	TLCSWY04	MMIC	80

Table 6.
Cost of available mm-wave RF components.
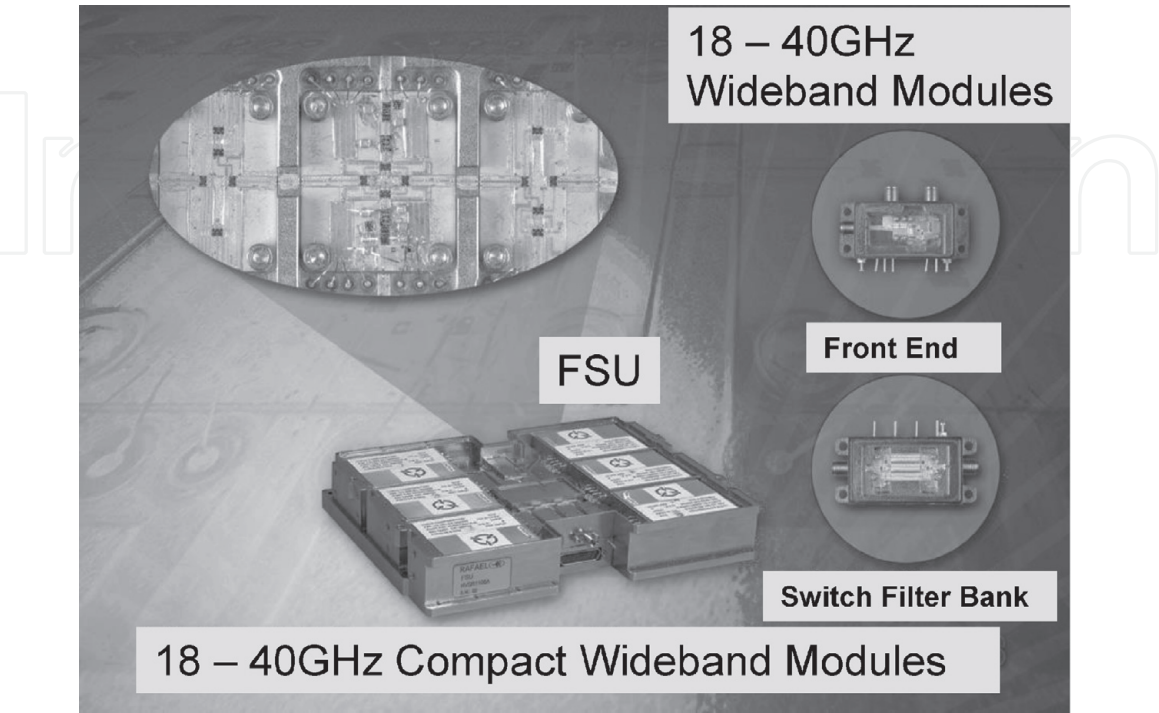
Figure 14.
Photo of 18–40GHz compact modules.

3. Wideband, 18 to 40 GHz, integrated compact switched filter Bank module

3.1 Introduction

Filter bank modules are an important module in direction finding, radar, seeker, and communication systems. The electrical performance of the filter bank determines if the system will meet the system-required dynamic range and signal-to-noise ratio (SNR) specifications. Moreover, in several cases the filter bank performance limits the system dynamic range. This section describes the design and development of an integrated, low-cost, 18 to 40 GHz wideband compact filter bank module. Design and fabrication considerations are presented.

The wideband SFB consists of three wideband side-coupled microstrip filters. The SFB MIMIC switches operate in the 18 to 40 GHz frequency range and are used to select the required filter. The insertion loss of each filter section is less than 11.5 dB $\pm$ 1.5 dB. The passband bandwidth of each filter is around 8 GHz. The received signal is rejected by 40 dB at ± 7GHz from the center frequency. The received signal is rejected by 60 dB at ± 11GHz from the center frequency. The SFB volume is 2 x 5 x 1 cm.

3.2 Description of the filter bank

Figure 15 presents the block diagram of the compact SFB unit. The SFB The module consists of three side-coupled microstrip filters. Each side-coupled filter consists of nine sections. The filters are printed on a 5-mil alumina substrate. One to two dB attenuators connect the filters input and output ports to wideband MMIC SPDT switches. The attenuators are used to adjust each channel's losses to the average required level. The module losses are adjusted to be higher in the low frequencies and lower in the high frequencies. The adjustment of the attenuation level improves the filters flatness over a wideband, 18–40GHz frequency range. The filters are assembled to the surface of the package metal box. The SFB switches are assembled on a CoVar carrier. In the development process of the SFB unit, we found
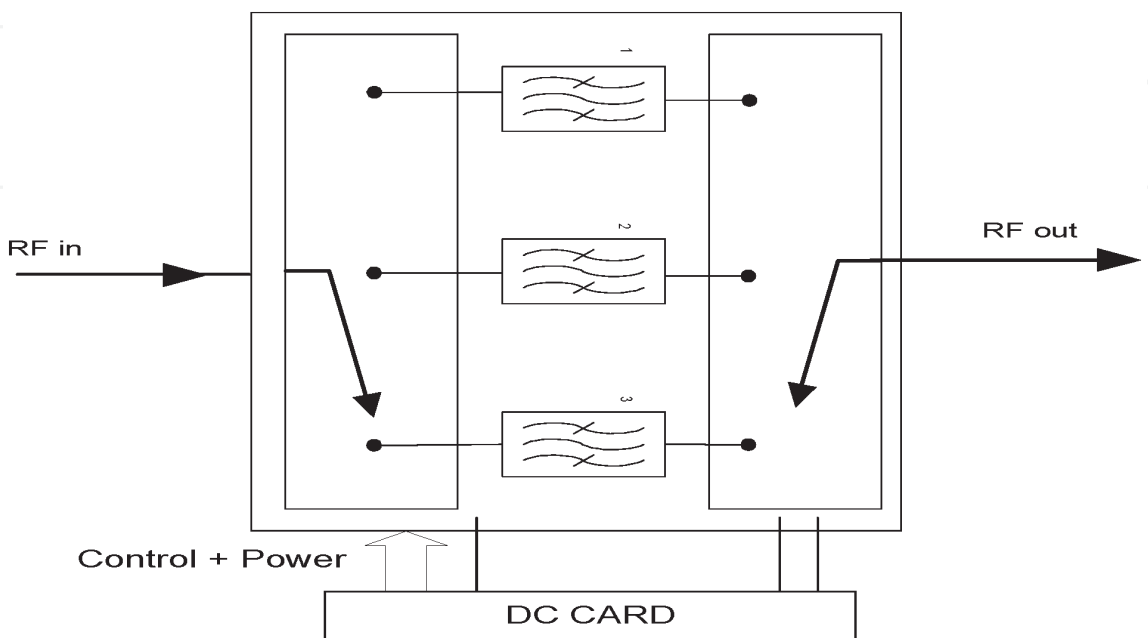
Figure 15.
Block diagram of the compact filter bank module.

that the spacing between the filter carriers and the switch carriers should be less than 0.03 mm to get S11 and S22 better than −9.5 dB and flatness better than ±1 dB.

3.3 Wideband switch filter Bank specifications

Table 7 lists the specifications of the wideband SFB.

3.4 Wideband filter design

The filters were designed by employing AWR and ADS software. **Figure 16** presents single filter response requirements. **Table 8** and **Figure 17** show the SFB expected frequency response. **Table 9** presents the advantages of the integrated design over the discrete design. For example, the weight of a discrete SFB is 1 kg and the weight of an integrated SFB is 50 g. The volume of the discrete SFB is twice the volume of the integrated SFB. The filter contains nine side-coupled microstrip lines printed on a 5-mil alumina substrate. ADS and AWR software were applied to optimize the filter dimensions and structure to meet the system requirements. **Figures 18**–**20** show the computed results of the filters. The sensitivity of the design to substrate tolerances such as height and dielectric constant has been optimized by using RF analysis software, see (**Figure 21**). We fabricated the filter configuration that was less sensitive to production tolerances (**Figure 24**).

Figure 22 presents computed S_{11} and S_{21} parameters for the SFB using ADS software. **Figure 23** presents the expanded S12 computed results of the filter bank. **Figure 24** presents the SFB board drawing. **Figure 25** is a photo of the SFB. **Figure 26** presents the S21 SFB results of the first unit measured during the production process. A comparison of the SFB computed and measured results proves that there is a good agreement between computed and measured results.

Parameter	Requirements
Frequency range	18–40.1 GHz
Number of channels	3
Channel Passband	8 GHz
Rejection	40 dB min @ F0 ± 8GHz
	50 dB min @
	F0 ± 11GHz
Flatness	± 1.2 dB max. For 4 GHz
I.L	12–14.5 dB
CH-1	10.5–13.5 dB
CH-2	9–12 dB
CH-3	
Switching time	100 nsec
Input Power	25 dBm max
VSWR	2.5:1 max
Control	2 LVTTL lines
Power Supply voltages	± 5 V DC. Heat dissipation – 1 W max
Dimension	5 x 2 x 1 cm

Table 7.
Wideband SFB specifications.
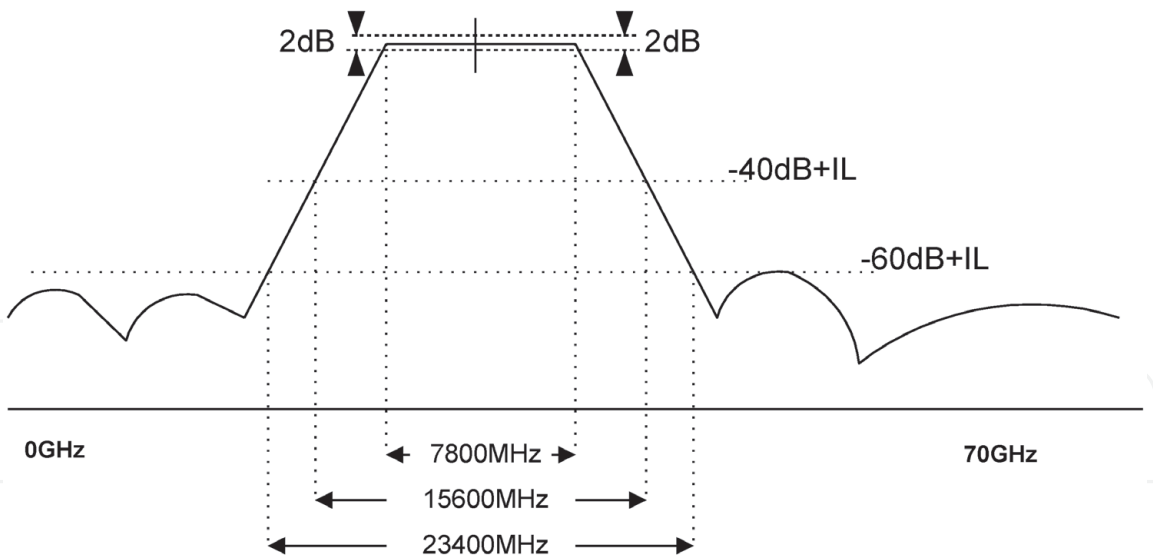
Figure 16.
Single filter response requirements.

CH	Rejection −60 dB	Rejection −40 dB	Passband −3 dB	Passband −3 dB	Rejection −40 dB	Rejection −60 dB
CH-1 (GHz)	10.1	14	17.9	25.7	29.6	33.5
CH-2 (GHz)	17.3	21.2	25.1	32.9	36.8	40.7
CH-3 (GHz)	24.5	28.4	32.3	40.1	44	47.9

Table 8.
SFB requirements.
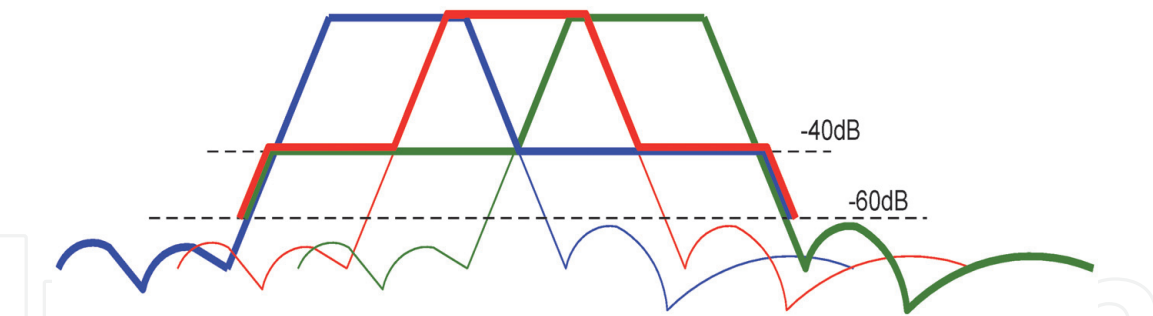
Figure 17.
SFB expected frequency response.

Parameter design	Dimension Cm	Weight Kg.	Price K$
Integrated	5.5 x 2.5 x 1.5	0.05	2.2
Discrete	12 x 6 x 3	1	10

Table 9.
Comparison between discrete and integrated design.

Figure 27 shows the measured S12 parameters of filter #2 during the production process. **Figure 28** shows the measured S12 parameters of the SFB during the production process. The SFB losses at high frequencies are around 9 dB and at the low frequencies the losses are around 9 dB (**Figure 28**). **Figure 29** presents the detailed measured S11 parameter of the SFB. **Figure 30** presents the detailed measured S12 parameter of the SFB.

CH-1 FILTER
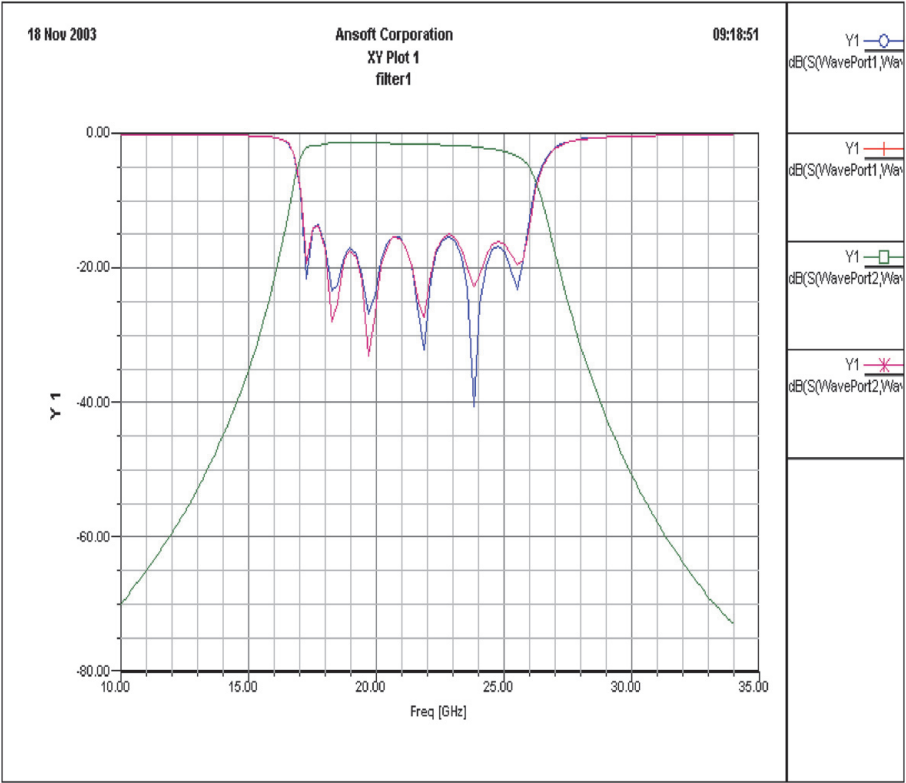
Figure 18.
S parameters for filter #1.

CH-2 FILTER
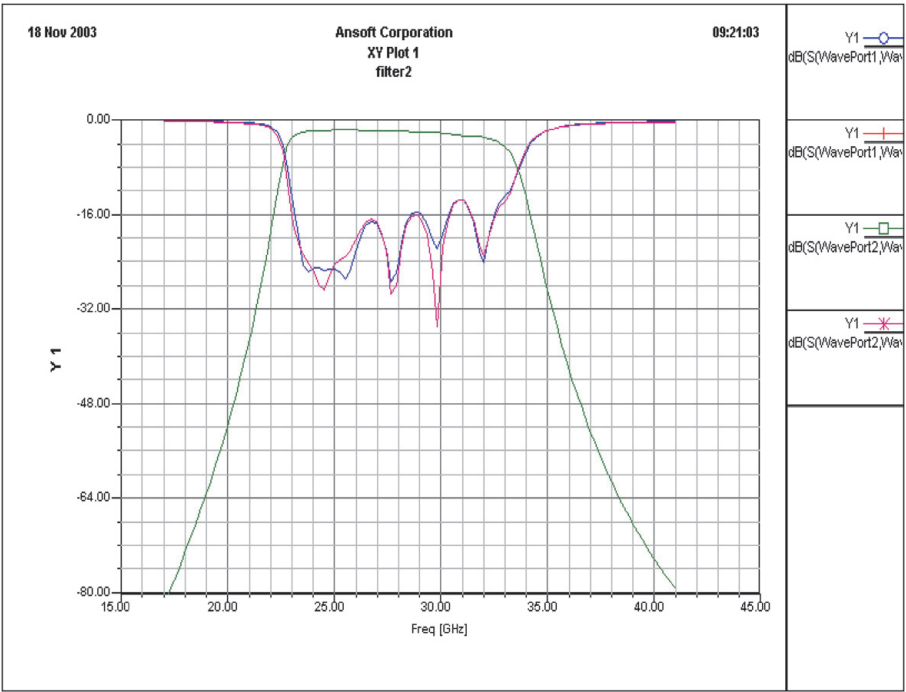
Figure 19.
S parameters for filter #2.

CH–3 FILTER
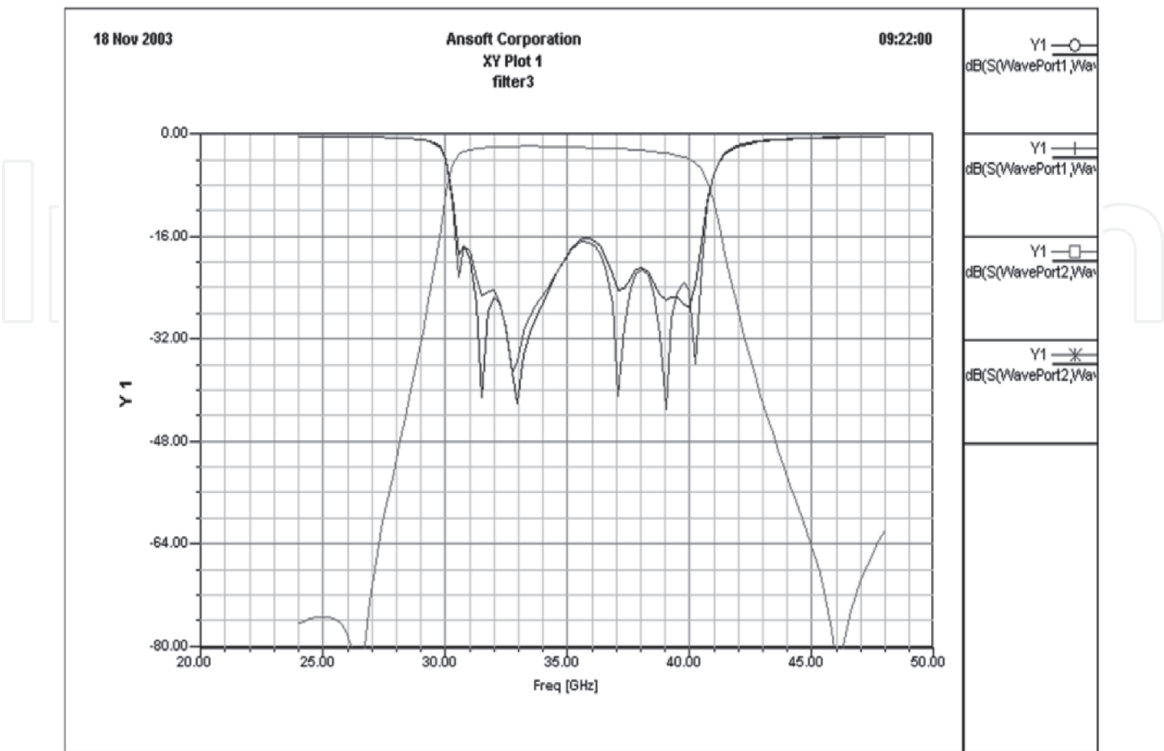
Figure 20.
S parameters for filter #3.

System1

		FILTER BANK		ATTENUATOR		SPDT		ATTENUATOR	
		Bessel Fo: 30000 BW: 8000 Gain: -3.01							Total
NF (dB)	2.00			1.00		2.00	1.00		9.01
Gain (dB)	-2.00			-1.00		-2.00	-1.00		-9.01
OIP3 (dBm)	30.00			30.00		30.00	30.00		20.32

Input Pwr (dBm)	-60.00	System Temp (K)	290.00	IM Offset (MHz)	.025
OIP2 (dBm)	16.42	OIP3 (dBm)	20.32	Output P1dB (dBm)	5.47
IIP2 (dBm)	25.43	IIP3 (dBm)	29.34	Input P1dB (dBm)	15.48
OIM2 (dBm)	-154.44	OIM3 (dBm)	-247.69	Compressed (dB)	0.00
ORR2 (dB)	85.43	ORR3 (dB)	178.67	Gain, Actual (dB)	-9.01
IRR2 (dB)	42.72	IRR3 (dB)	59.56		
SFDR2 (dB)	45.68	SFDR3 (dB)	63.52	Gain, Linear (dB)	-9.01
AGC Controlled Range:		Min Input (dBm)	N/A	Max Input (dBm)	N/A

Figure 21.
SFB analysis results.

4. Wideband MM-Wave Couplers

Couplers are used to couple part of the power in the input port to a coupled port. For example, as presented in **Figures 8** and **9**. Usually couplers consist of two coupled quarter-wavelength transmission lines and have four ports, as shown in
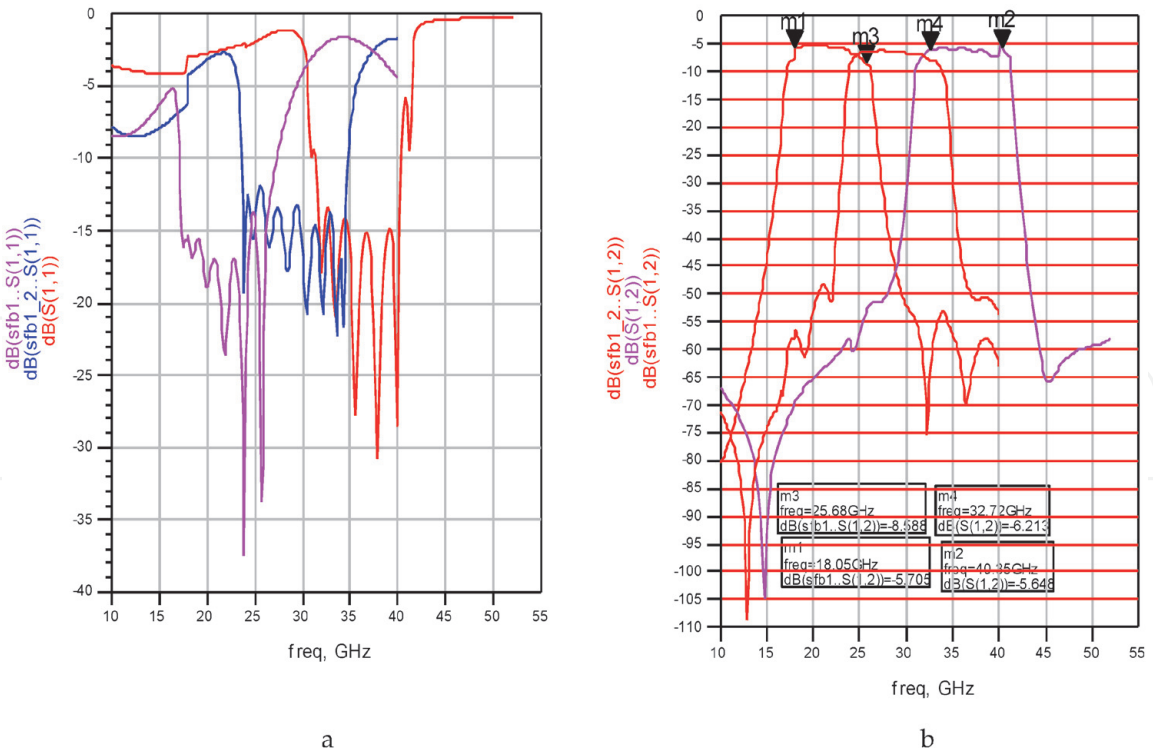
Figure 22.
a. S_{11} SBF computed results; b. S_{21} SBF computed results.
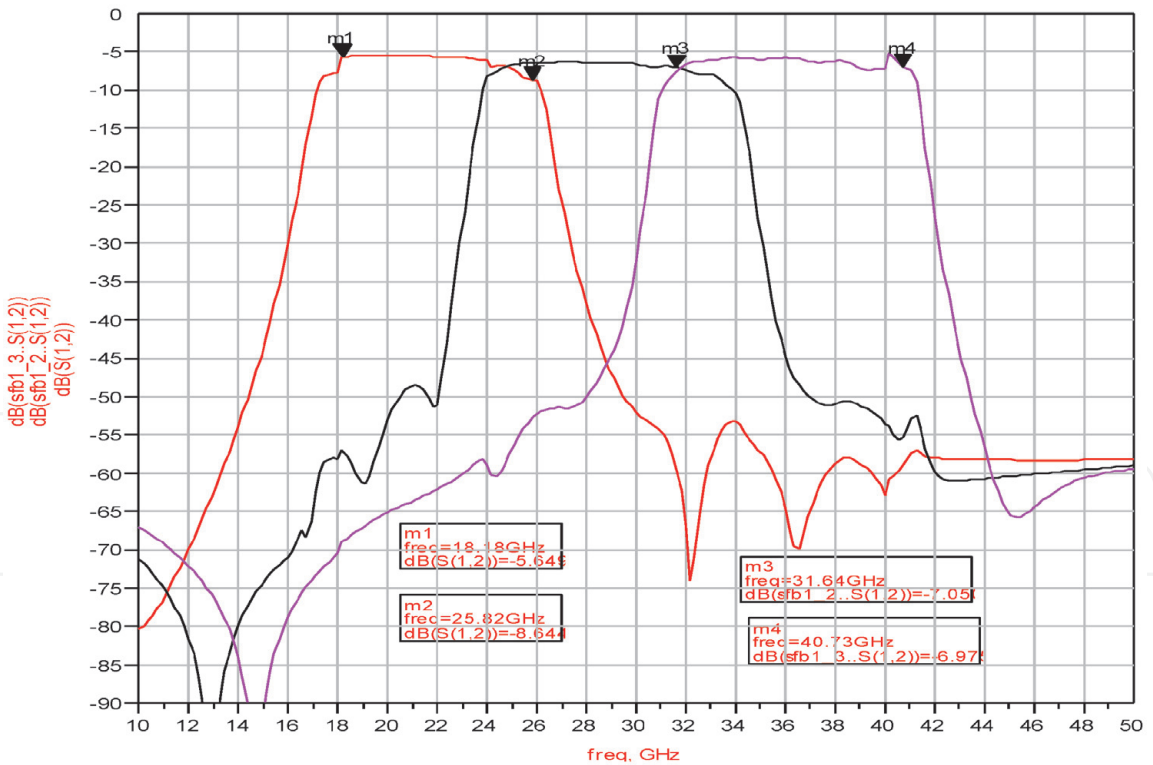
Figure 23.
SFB S12 computed results.

Figure 31. P1 is the input port, P2 is the transmitted port, P3 is the coupled port, and P4 is the isolated port. The coupled port may be used to obtain the information about the signal such as frequency and power level without interrupting the main power flow in the device. The coupling factor may be calculated by using Eq. (1) and is the ratio between the coupled power to the input power in dB when the other ports are terminated. Coupler losses may be calculated using Eq. (2). The overall
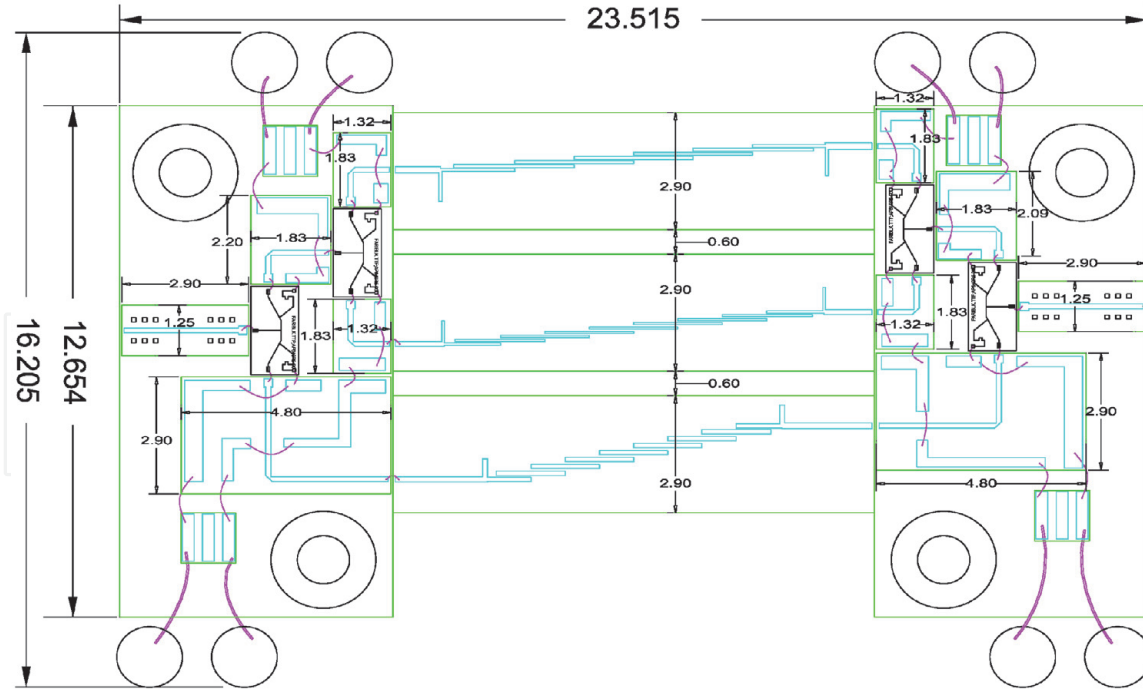
Figure 24.
SFB layout.
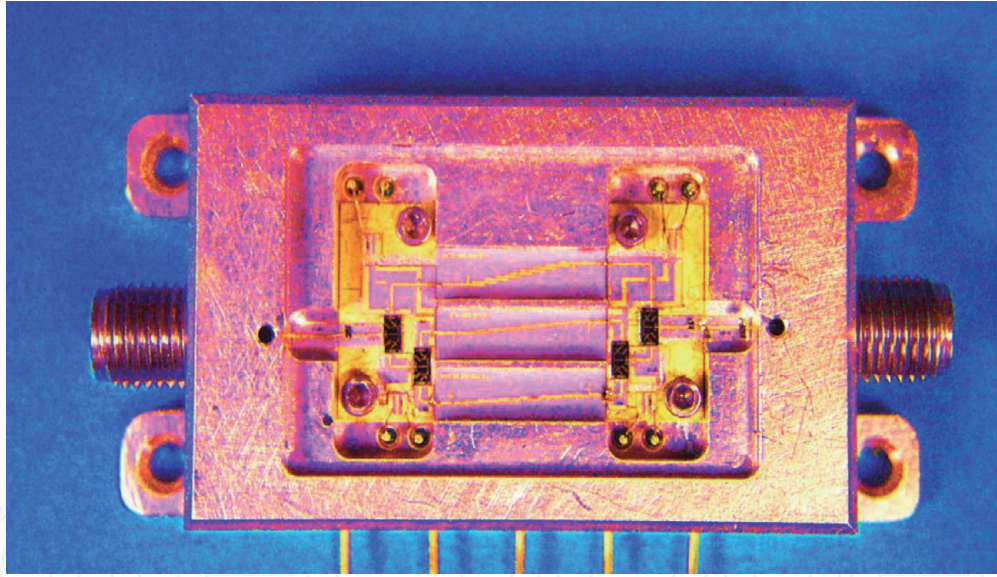
Figure 25.
SFB picture.

coupler losses are due to conductor losses, coupling losses, dielectric losses, radiation losses, and matching losses.

$$Coupling\ Factor = CF = -10\,log\,\frac{P3}{P1} \tag{1}$$

$$Insertion\ Loss = IL = 10\,log\left(1 - \frac{P3}{P1}\right) \tag{2}$$

The isolation factor is the ratio between the power in the isolated port to the input power in dB when the other ports are terminated and is given by Eq. (3).

$$Isolation = -10\,log\,\frac{P4}{P1} \tag{3}$$
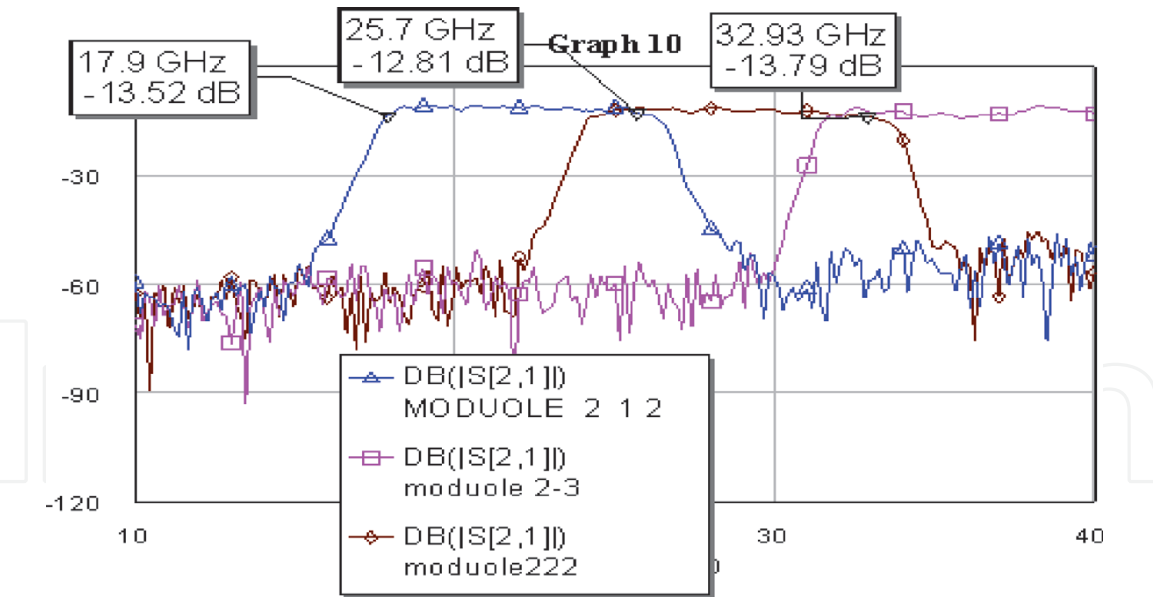
Figure 26.
SFB measured results unit number 1.
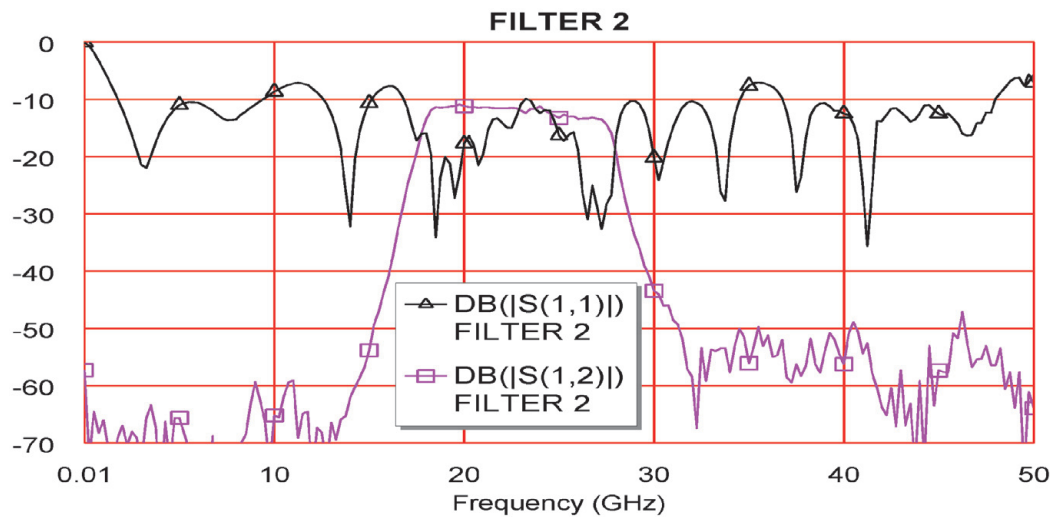
Figure 27.
Measured S parameters for filter #2.
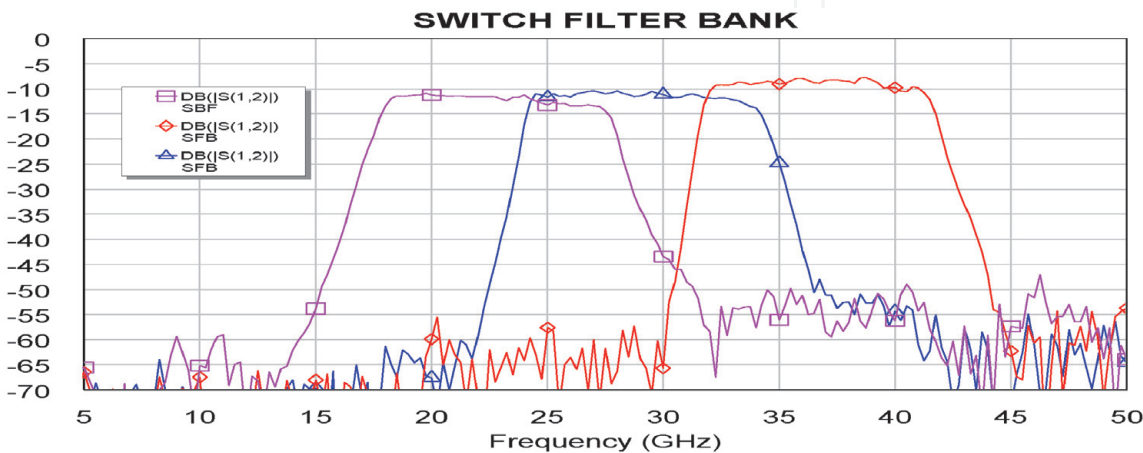
Figure 28.
SFB measured S12 results.

19
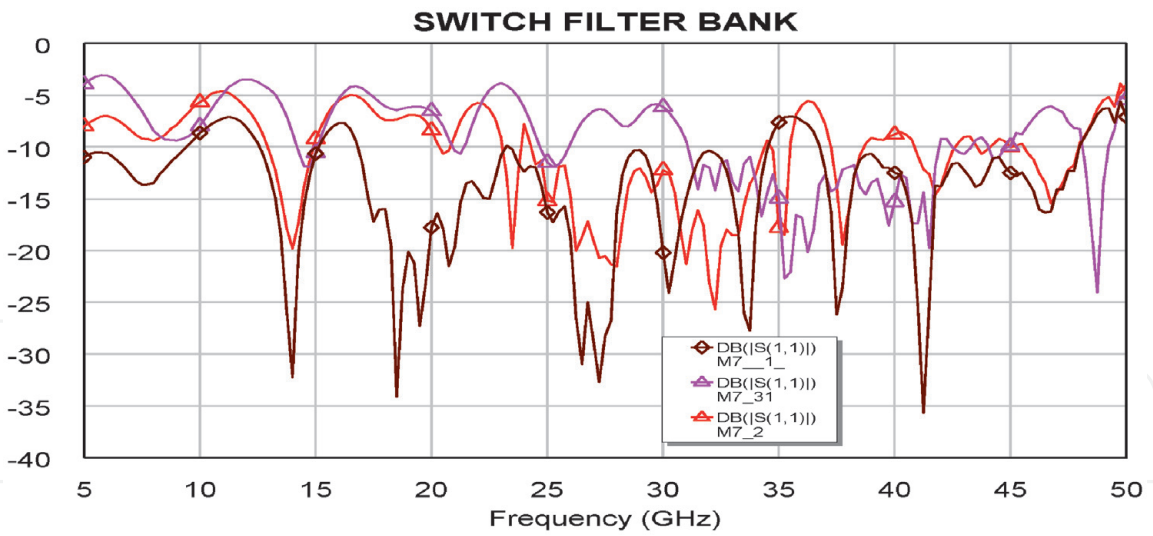
Figure 29.
SFB measured S11 results.
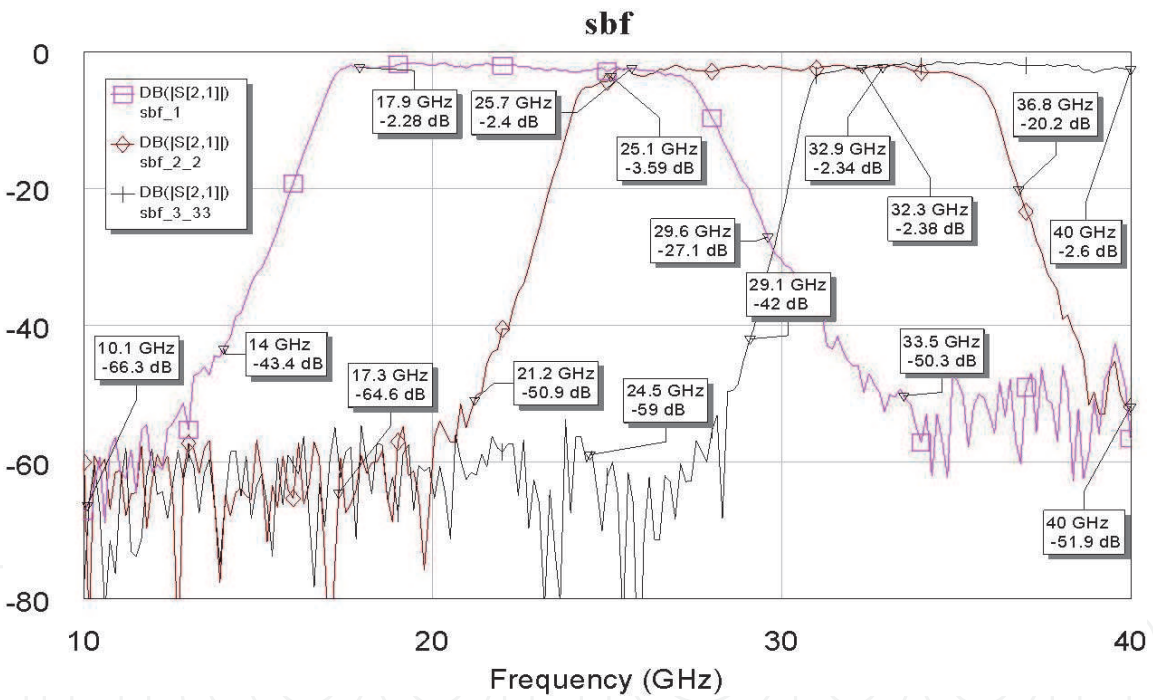
Figure 30.
SFG detailed measured S12 results.
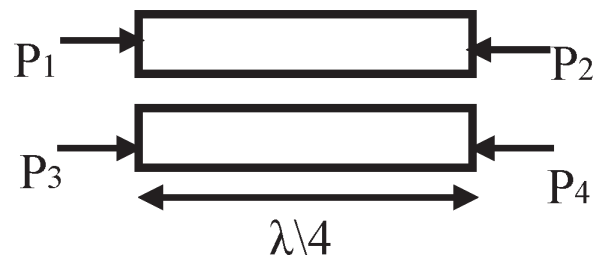
Figure 31.
Coupled lines.

The coupler directivity is the ratio between the power in the isolated port to the coupled power in dB when the other ports are terminated and is given by Eq. (4).

$$Directivity = D = -10 \log \frac{P4}{P3} \tag{4}$$

In radars, DF systems, seekers, and communication systems, the amplitude and phase balance between the system ports determines the accuracy of the signal processing process. The power difference in dB between two output ports of the system is defined as the amplitude balance. In an ideal hybrid circuit, the amplitude difference between two ports should be 0 dB. The phase difference in degrees between two output ports of the system is defined as the phase balance. However, in real life the amplitude balance and phase balance vary with frequency.

4.1 A wideband MM-wave coupler

Figure 32 presents a wideband MM-wave coupler printed on alumina with a 9.8 dielectric constant and 5.5 mil-inch thickness. The coupler frequency range is 18 GHz to 40 GHz. The coupler was designed by Momentum ADS software. The coupling value is −13 dB and is shown in **Figure 33**. The coupler insertion loss is 0.4 dB and is shown in **Figure 34**. The coupler S11 parameter is better than −26 dB and is shown in **Figure 35**.
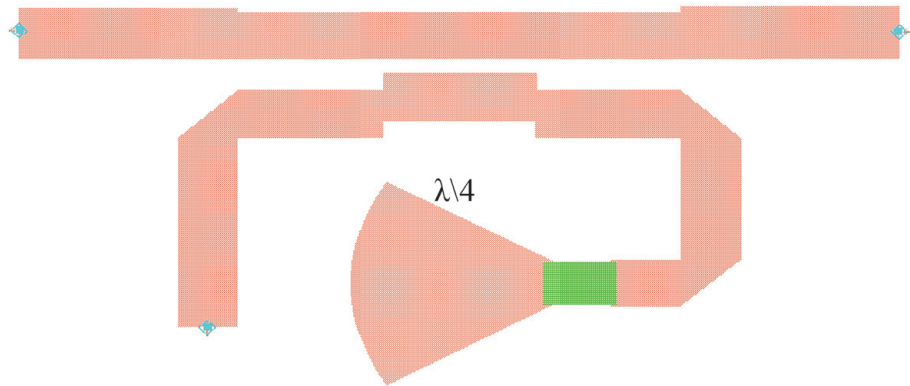

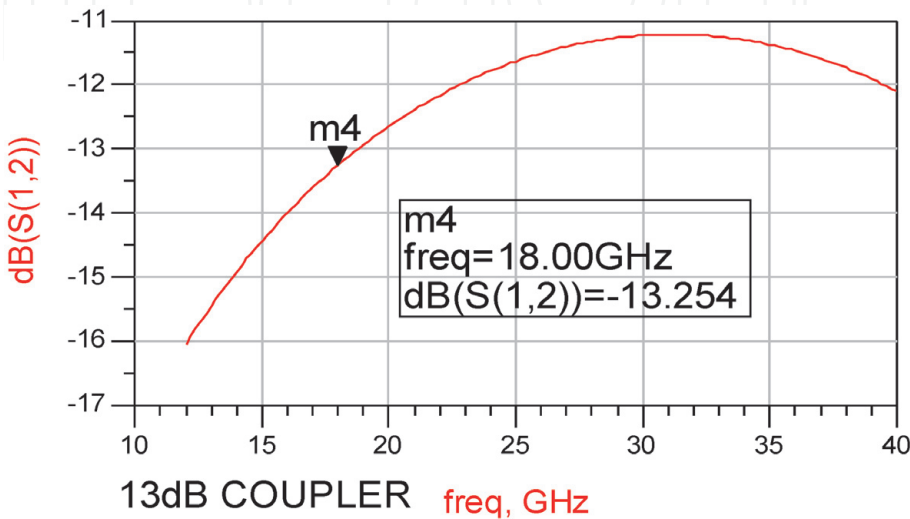**Figure 32.**
18 GHz to 40 GHz, wideband MM-wave coupler.

Figure 33.
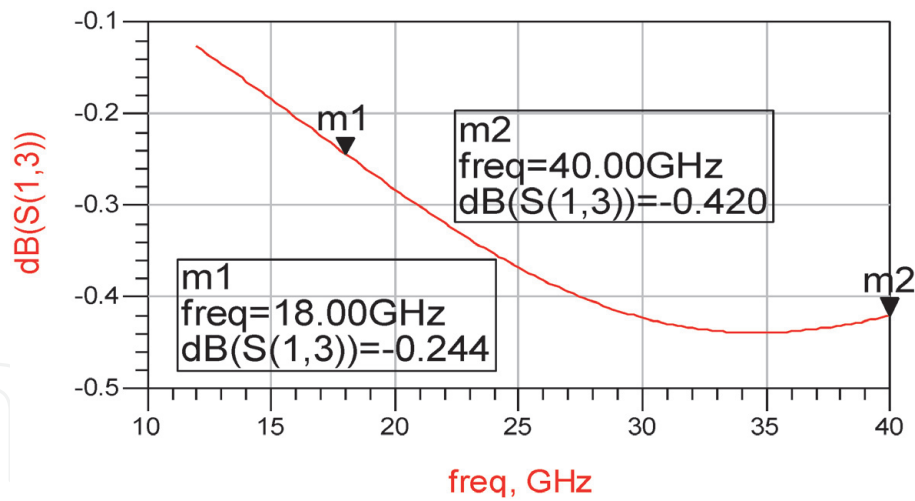*The wideband coupler coupling value, S12.*

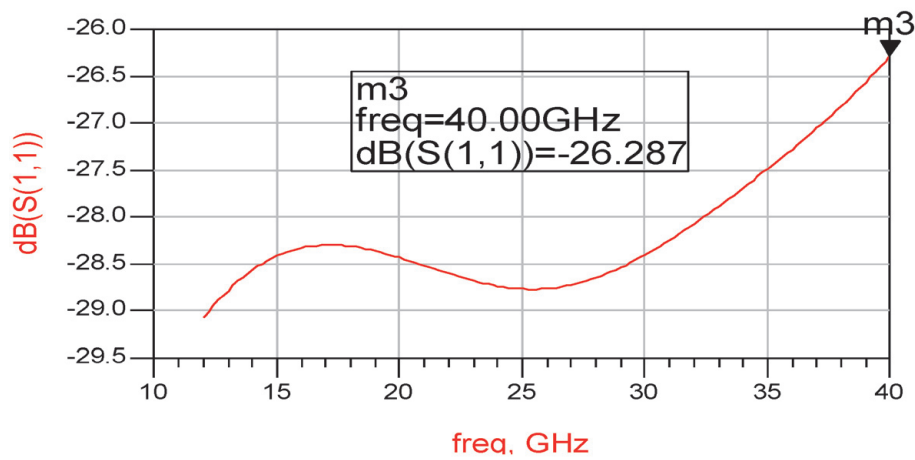**Figure 34.**
The wideband coupler insertion loss.

Figure 35.
S11 of the wideband coupler.

5. Conclusions

This chapter presented a low-cost, integrated 18–40 GHz wideband compact frontend with a 47 dBm high power limiter. The frontend consists of two channels: a high gain and low gain channel. Wideband MMIC switches are employed to select the required channel. The gain of the high gain channel is around 27 dB with ±1 dB flatness. The noise figure of the module is around 9 dB.

This chapter also discussed the design and performance of a compact, low-cost, integrated SFB. The integrated SFB has several advantages over the discrete SFB. For example, the weight of a discrete SFB is 1 kg and the weight of an integrated SFB is 50 g. The volume of the discrete SFB is twice the volume of the integrated SFB. The filter contains nine side-coupled microstrip lines printed on a 5-mil alumina substrate. ADS and AWR software were applied to optimize the filter dimensions and structure to meet the system requirements. The filter's passband bandwidth is around 8 GHz. The SFB insertion loss is around 12 dB in the low frequency range and 9.5 dB in the high frequency range. The filter flatness in the passband frequencies is better than ±1 dB. The received signal is rejected by 40 dB at ±7 GHz from the center frequency. The received signal is rejected by 60 dB at ±11GHz from the center frequency. The SFB volume is 2 x 5 x 1 cm.

Author details

Albert Sabban
Kinneret College, Kinneret Israel and Ort Braude College, Karmiel, Israel

*Address all correspondence to: sabban@netvision.net.il

IntechOpen

References

[1] J. Rogers, C. Plett "Radio frequency Integrated Circuit Design", Artech House, 2003.

[2] N. Maluf, K. Williams, "An Introduction to Microelectromechanical System Engineering", Artech House, 2004.

[3] Albert Sabban (2016). "Wideband RF Technologies and Antenna in Microwave Frequencies", Wiley Sons, July 2016, USA.

[4] Albert Sabban Editor and Author (2020). Wearable Systems and Antennas Technologies for 5G, IOT and Medical Systems CRC PRESS, TAYLOR & FRANCIS GROUP, December 2020. ISBN 9780367409135.

[5] Albert Sabban (2017). "Novel Wearable Antennas for Communication and Medical Systems", TAYLOR & FRANCIS GROUP, October 2017.

[6] Albert Sabban (2015). "Low visibility Antennas for communication systems", TAYLOR & FRANCIS GROUP, 2015, USA.

[7] S. A. Mass, "Nonlinear Microwave and RF Circuits", Artech House, 1997.

[8] Abdeen Hebat-Allah Yehia; Yuan Shuai; Schumacher Hermann; Ziegler Volker; Meusling Askold; Feldle Peter. "10 to 40 GHz Superheterodyne Receiver Frontend in 0.13 μm SiGe BiCMOS Technology". Frequenz, Volume 71, pp.151-160. March 2017.

[9] A. Sabban, "Microstrip Antenna Arrays", 2011, Microstrip Antennas, Nasimuddin Nasimuddin (Ed.), ISBN: 978-953-307-247-0, InTech, pp. 361-384,

[10] A. Sabban, "Applications of MM Wave Microstrip Antenna Arrays" ISSSE 2007 Conference, Montreal Canada, August 2007.

[11] Reuven Shavit, Albert Sabban, Michael Sigalov, Avihai Lahman, Zeev Iluz, Naftali Chayat and Solon Spiegel "microwave engineering research activity in Israel", IEEE Microwave Magazine, May 2018, 19(3):129-135. DOI: 10.1109/MMM.2018.2802281

[12] G.P. Gauthier, G.P. Raskin, G.M. Rebiez., P.B. Kathei, "A 94GHz Micro-machined Aperture- Coupled Microstrip Antenna", I.E.E.E Trans. on Antenna and Propagation Vol. 47, No. 12, pp. 1761-1766, December 1999.

[13] G. de Lange et. al., "A 3*3 mm-wave micro-machined imaging array with sis mixers", Appl. Phys. Lett. 75 (6), pp. 868-870, 1999.

[14] A. Rahman et. al., "Micro-machined room temperature micro bolometers for MM-wave detection", Appl. Phys. Lett. 68 (14), pp. 2020-2022, 1996.

[15] A. Sabban and K.C. Gupta, "Characterization of Radiation Loss from Microstrip Discontinuities Using a Multiport Network Modeling Approach", I.E.E.E Trans. on M.T.T, Vol. 39, No. 4, April 1991, pp. 705-712.

[16] Keysight software, http://www.keysight.com/en/pc-1297113/advanced-design-system-ads?cc=IL&lc=eng